Vapor-sorption Coupled Diffusion in Cellulose Fiber Pile Revealed by Magnetic Resonance Imaging

Xiaoyan Ma, Benjamin Maillet, Laurent Brochard, Olivier Pitois, Rahima Sidi-Boulenouar, Philippe Coussot

Vapor-sorption coupled diffusion in cellulose fiber pile (fabric) revealed by MRI

X. Ma, B. Maillet, L. Brochard, O. Pitois, R. Sidi-Boulenouar, P. Coussot

Laboratoire Navier (Ecole des Ponts Paris Tech-Univ Gustave Eiffel-CNRS), Champs-sur-Marne, France

Abstract: Moisture transport and/or storage in clothes plays a major role on the comfort or discomfort they procure due to the resulting wetness or heat loss along the skin. Our current knowledge of these complex processes which involve both vapor transport and water sorption in the solid structure, is limited. This is in particular due to the open questions concerning the sorption dynamics at a local scale (for modelling), which lead to complex non-validated models, and to the challenge that constitutes the direct observation of these transports (for measurements). Here, through unique experiments, we directly observe the bound water transport in a model textile sample during drying with the help of an original Magnetic Resonance Imaging (MRI) technique. Despite the various physical effects involved this transport appears to follow a diffusion-like process. We then demonstrate theoretically that this process is described in details (at a local scale) by a simple model of vapor transport through the structure assuming instantaneous sorption equilibrium and without any parameter fitting, which finally brings a simple response to modelling. This in particular allows to quantify, as a function of simply measurable material parameters and air flux impact, the characteristic time during which the evaporation of sweat is accelerated by sorption, the time during which a textile constitutes a barrier against ambient humidity, or the conditions of mask humidification. These results open the way to a full characterization and prediction of fabric properties under different conditions, and to direct formulation of high performance materials by adjusting the material constituents.

I. INTRODUCTION

Evaporation of wetness, usually sweat, is crucial in human thermoregulatory function. Clothing constitutes a protection against external conditions but it also usually stores humidity from sweat or ambient humidity. One of the factors considered as the most crucial in causing wear discomfort during physical activity is the presence of wetness at the skin-clothing interface [1-4] but, thanks to water sorption in fabric, clothing can also play a significant role in the moisture transport or storage [1], and heat loss due to sweating [5] as water vapor adsorption is an exothermic process. An analogous problematic exists with bio-based materials used for construction such as wood, hemp concrete, etc, which appear as excellent hygrothermal regulators [6-7]. On another side, the drying of textiles requires a huge amount of energy and the search for the most efficient technique is a critical stake [8]. At last, the question of the impact of humidification, due to humid exhaled air, on the efficiency of masks against COVID-19 propagation or severity, is critical [9-10].

The current description of these processes relies on empirical models [11-12], global laws [1, 13-16] or statistical approaches [17], of limited applicability, for describing vapor or heat transfers through fabrics. For example, the mass flux of water evaporating from a surface covered by a textile is often considered to be simply proportional to the vapor pressure difference and to a material coefficient, i.e. the so-called “clothing vapor resistance” [12, 14-15]; an approach which is likely valid in steady state. The heat transfer is then assumed to be simply proportional to this vapor mass flux. On another side, an empirical (negative) exponential model was suggested to represent the moisture content vs time during drying of viscose bobbins, with parameters depending on temperature, bobbin diameter, volumetric flow rate, etc [11].

Alternatively, sophisticated models have been developed, starting with Henry [18] then followed by [19-26], which take into account at best all the internal processes (vapor transport, sorption, etc), but they generally involve various a priori unknown parameters. The predictions of these models appear to be in qualitative agreement with observations but can hardly be fully validated due to the absence of appropriate measurements of internal physical quantities.

One of the major complexity in the process analysis lies in the fact that hygroscopic fabrics such as wool, viscose, cotton, silk, nylon, some polyesters, etc, contain some significant amount of water which can be absorbed by the solid structure from vapor in the surrounding air. The transfers of this so-called bound water play a fundamental role in the humidity control

and feeling. However, following the transport of bound water in such materials remains challenging. This in particular leaves the pivotal question of the role of sorption dynamics open, and leads to various speculations in models.

The complete modelling approaches first rely on the conservation of water vapor mass while it diffuses through the structure, taking into account the loss or contribution due to sorption or desorption. The second equation, which expresses the conservation of heat, has a similar form, with a term associated with latent heat due to sorption or desorption. Thus the sorption or desorption processes play a critical role in these equations, both on the mass transfer and heat transfer (through latent heat), and they are also the main unknown in these equations. In his pioneering modelling work, Henry [18] suggested that sorption or desorption should be considered as instantaneous, but subsequent models generally assumed the opposite and attempted to describe the sorption dynamics in details, which led to various speculations. David and Nordon [26-27] assumed the rate of mass transfer to be proportional to the difference between current and equilibrium relative humidity, with a factor expressed as an exponential function of the difference between these two relative humidities. Then, in a series of works by Li and co-authors [21-25] it was suggested that the sorption process should be described by a two-stage sorption rate equation. Here, the first stage is represented by a Fickian diffusion with constant diffusion coefficient; the second-stage sorption follows an exponential relationship. The relative contributions of the two stages to the total uptake vary with the stage of sorption and the initial regain of the fibers.

On another side, biobased construction materials are also porous hygroscopic media which can absorb a significant fraction of bound water. Some fiberboard materials used for insulation exhibit characteristics resembling that of textile. Numerical hygrothermal models [28-30] have been developed in literature which take into account at best internal processes (vapor transport, sorption, etc), but they also generally involve some unknown parameters concerning the sorption-desorption dynamics. Finally, significant discrepancies subsist between the predictions of these models and macroscopic measurements [31-32], suggesting the need of progress concerning the physical process description in these models.

Here, with the help of a specific Magnetic Resonance Imaging sequence which makes it possible to measure the local full amount of bound water at any time throughout the sample, we directly observe the bound water transport in a model textile sample (cellulose fiber pile) during drying. It appears that its transport essentially follows a simple diffusion-like process. We then show that this transport is described in details (at a local scale) by a simple model of vapor transport through the structure assuming instantaneous sorption equilibrium. The agreement between the model predictions without any fitting parameter and the internal data in time fully supports the model validity. This model makes it possible to predict the rate at which bound water is extracted or stored, and the corresponding heat exchange rate. These results open the way to a full characterization and prediction of material textiles properties under different conditions, and to direct formulation of high performance materials by adjusting the material constituents.

II. FOLLOWING BOUND WATER IN A DRYING MODEL TEXTILE

A. Materials

We use cellulose, which is used for various fabrics, and can be considered as a model textile material. In particular its sorption isotherm appears to have a shape qualitatively similar to that of other textile materials such as silk, cotton, wool, viscose, nylon, with a typical Moisture Content (MC) (i.e. water to solid mass ratio) reaching 20-30% at high relative humidity [33], i.e. the so-called Fiber Saturation Point. The material was made of pure (99.5%) cellulose fibers (*Arbocel BC1000*, supplied by Kremer Pigmente). These fibers are hydrophilic and essentially made of natural crystalline cellulose. The average fiber thickness is 20 µm and the average length is 700 µm. The bulk fiber density is about 1500 kg/m^3. Sorption isotherm was performed at room temperature (22$\pm$2°C). Cellulose samples were first dried in an oven of 60°C for 3 days, which sets up at a low moisture content (with a small amount of residual bound water, likely of the order of 0.5% in terms of moisture content). Note that we used this state as the reference one for supposedly dried state. Then different samples were placed in desiccators with different salt solutions or a bath of deionized water imposing different RH (Relative Humidity) values at equilibrium. The MC of the cellulose sample upon adsorption was then measured at equilibrium. By following the sample mass in some cases we could check that a plateau in mass was reached after about one week, so we left the samples between 2 and 3 weeks to be sure to get the equilibrium state. The MC for desorption was measured at equilibrium from samples prepared

through the above sorption procedure (up to equilibrium) then placed at a lower RH imposed by salts. The sorption-desorption data show a typical aspect with a slow initial increase as a function of RH followed by a fast increase of the MC at the approach of the maximum RH (see Figure 1). Remarkably the data for sorption and desorption are very close. Hysteresis in sorption-desorption measurements are generally due to capillary effects and can be significant for sufficiently small pores (say, <50 nm). The absence of hysteresis confirms that such small pore size is negligible within this porous structure made by the entanglement of fibers of much larger characteristic length (more than a few hundreds of microns). This is then again confirmed by our NMR measurements. Hysteresis in nanopores, in particular in cellulose, may also result from adsorption-swelling coupling [34]. The absence of hysteresis in our case suggest that such effects are absent and/or our equilibration time was sufficiently large.

Note that we also will see below that this MC includes a negligible amount of free water in pores.

These data can be very well represented by the following empirical model:

$$s = 0.106n + \left(n/1.33\right)^8 \qquad (1)$$

in which s is the MC and n the RH.

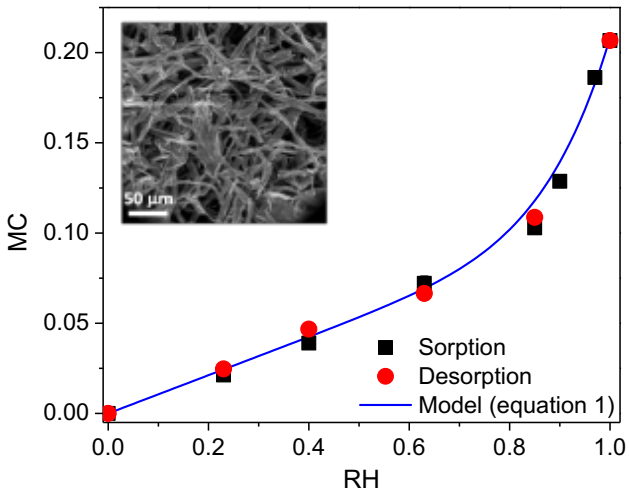

Figure 1. Sorption and desorption data for cellulose fibers. Each data point was obtained by averaging independent measurements obtained on at least three different samples. The error bars are within the symbol size. The inset shows an ESEM Image of the cellulose structure (from [29], N. Ben Abdelouahab courtesy).

The cellulose samples for drying tests are prepared by mixing them manually and gently packing the resulting material in a glass cylindrical cup, so that only the top surface is in contact with air. The sample size was 7 mm diameter and 10 mm thick for NMR tests, 60 mm diameter and different thicknesses for macroscopic (weighing) and MRI tests. The apparent porosity of the samples is $82 \pm 1\%$, but due to the large deformability of this material the local concentration could not be perfectly controlled, so that there may subsist some slight heterogeneities (see below). These samples are then kept in desiccator at high RH for several weeks. The initial MC of the samples for MRI tests was 18% (97% RH), while the other samples were saturated (21% MC, 100%RH).

B. Drying set up

We induce a constant dry air flux (relative humidity below 0.5%) vertically against the sample free surface (see Figure 2) and we follow the water amount in time with NMR for 1 cm samples or MRI for the thickest samples (see below). The tests carried out with these techniques were reproduced outside the magnet, by imposing similar air flux and weighing the sample in time. This allowed to check the ability of our NMR and MRI measurements to properly follow the (non-vapor) water mass in time (see Appendix 1). We also carried out additional tests by only weighing the samples during drying. However, following the sample weight under an air flux provides data with more scatter due to the air flux pressure on the balance, whose relative impact is larger for lower sample weight. In contrast, NMR measurements strictly reflect the internal water content whatever the mechanical constraints on the sample and, for these light cellulose samples, directly provide precise mass vs time curves (see below and Appendix 1).

Note that the air flux is obtained from a tube whose exit is at some distance from the sample surface. Both this distance and the air flux velocity can be tuned, and the resulting air flux along the sample surface also depends on the geometry of the whole set up. This finally mainly induces an air flow tangentially to the upper surface of the sample. As we will see later, the resulting drying rate can be fully characterized by a single parameter, namely a characteristics distance of vapor diffusion from the sample free surface, so that it is useless to describe in details the air flux characteristics. For example, for the experiments for which this characteristics distance (δ) is 8 mm, the tangential air flux velocity at about 1 cm above the sample is of the

order of 10 cm/s, which would correspond to a weak wind.

In practice, textile drying occurs under a variety of conditions. In laboratory, the evaporation properties may be studied under some ambient humidity without controlling precisely the air flux [5], or with a tangential motion of the fabric with respect to ambient air [1, 15]. In some cases the motion of a person wearing clothes is considered [12]. Thus, depending on the conditions a purely tangential flow, or a more complex flow involving tangential and normal components, are considered. Actually, whatever the characteristics of the flow at some distance from the sample surface, the flow close to this surface is necessarily tangential; then we can expect vapor diffusion in the direction perpendicular to this surface at least over some thickness, with possible perturbation beyond; but in steady state the resulting drying rate can still be described with the help of an equivalent thickness (i.e. δ, see below) of diffusion of vapor in open air.

This thickness will vary as a function of the exact flow conditions and sample geometry. For example, during this work we could observe that δ is significantly larger (i.e. slower drying rate) for an air flux tangential to the sample surface than for the same air flux but (at some distance) normal to the free surface.

Thus, the present work is easily applicable for any given homogeneous air flux conditions along the sample surface, so that main transport processes are perpendicular to the sample surface. The situation is more complex when a sample, or a clothes, is subjected to different air fluxes at different positions of its surface. In that case we can expect different evolutions of moisture content depending on the position, and possible transversal diffusion processes not taken into account here.

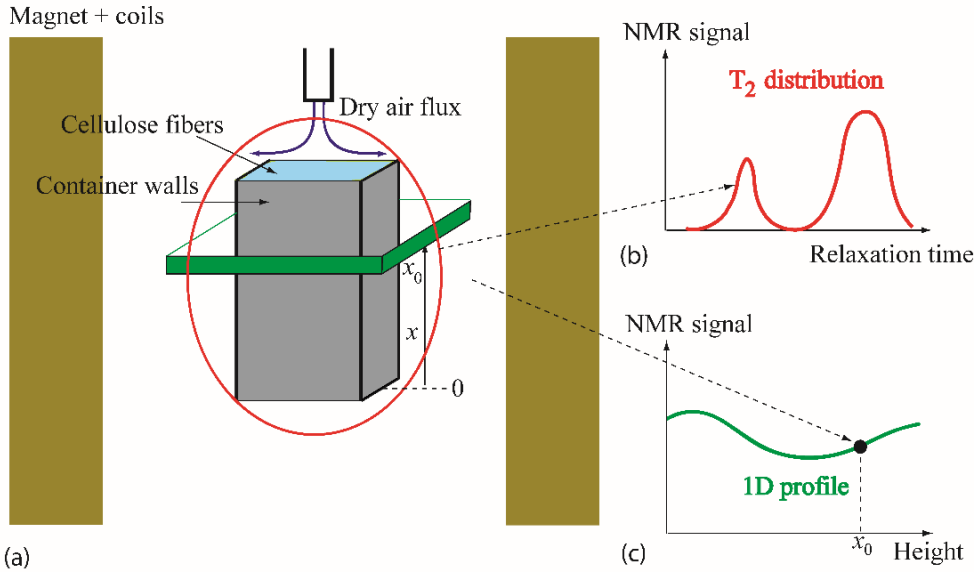

Figure 2: Scheme of the experimental set up with the sample inside the magnet (a), and main NMR (T_2 distribution) (b) and MRI (1 D profile) (c) sequences used to explore the water content during sample drying.

C. Bound water measurement by NMR and MRI

For sufficiently thick samples we measured the distribution of moisture content along the sample vertical direction during a drying test by means of the Single Point Imaging sequence (SPI). This sequence is dedicated to the study of materials with very short spin–spin relaxation times, generally shorter than 1 ms. Since cellulose samples contain mostly bound water whose relaxation time further decreases when the water content decreases, this sequence is well adapted to follow the moisture content, especially at the ultimate stages of drying. The distribution of water in small cross-sectional layers along the sample height direction (see Figure 2c), which we also call a profile, is obtained at different times. It is noticeable that the measured profiles are also sensitive to the geometry of the sample confined in the container. That is why there could appear ramps (or curvature) on the bottom border of the profiles. A more detailed description of the MRI sequence is provided in an earlier study [35]. Here we used a flip angle of 50° with a repetition time of 40 ms. The measurement time was 380 µs, of the order of the relaxation time of bound water in cellulose.

The whole profiling process was repeated 64 times on purpose of phase cycling and signal accumulation, and lasted about 6 min. The resolution was 0.78 mm. The mass of cellulose is recorded before and after the drying test, therefore the NMR signal can be calibrated on the effective mass loss.

With 1 cm-thick samples we measured the NMR relaxation through a Carr-Purcell-Meiboom-Gill (CPMG) [36] sequence composed of a first π/2-pulse and a train of π pulses during 160 ms. The echo time is 0.4 ms and the echo number 400. The repetition time is 1 s to get a complete relaxation of all protons. This sequence is repeated 128 times to increase the signal to noise ratio. The duration of the measurement is 3 min. This technique provides us with a set of data representing the complete relaxation of the NMR signal from all water molecules in the sample. However, the relaxation time of these molecules depend on their mobility, which typically decreases when the water is contained in smaller pores. We thus expect different values of this relaxation for different molecules in the sample. The distribution of T_2 values can then be resolved by means of ILT (Inverse Laplace Transform). Our procedure is a non-negative least square fit to the data with Tikhonov regularization; it is similar to the 'Contin' method [37-38], and is described in [39]. We finally get an apparent probability density function of T_2, expressed in terms of signal intensity associated with each possible value of T_2 (see Figure 2b)

For the NMR tests we integrate the relaxation time distribution to get the current water mass. For the MRI experiments we integrate the NMR signal over each profile to get the current water mass. We can remark that in both cases there is an apparent residual amount of NMR signal after the end of drying (indicated by a plateau of the apparent mass). The corresponding mass is only partly withdrawn after oven drying. This suggests that after the end of the test there remains a small fraction of water inside the sample because the air flux RH was not exactly 0%, and a fraction of hydrogen protons in the (dry) cellulose structure providing some residual NMR signal; in each case these amounts are equal to a few percent of the total water mass. In order to strictly follow the bound water fraction which is "mobile" within the frame of our tests, we subtract, from the mass and from the profiles, the value associated with the total residual signal.

III. GENERAL CHARACTERISTICS OF BOUND WATER EXTRACTION

Typical aspect and evolution of the relaxation time distribution, as obtained from NMR relaxometry during the drying of a cellulose sample initially filled with bound water, are shown in Figure 3. We initially observe essentially one peak around 3 ms. Such a small time value is characteristic of bound water in cellulosic material such as wood (see [40-41]). During drying this peak progressively shifts towards about 1 ms. This means that all along the process we measure mainly bound water, i.e. there is no condensation of capillary water. This progressive shift results from a loss of mobility of the bound water as its concentration decreases.

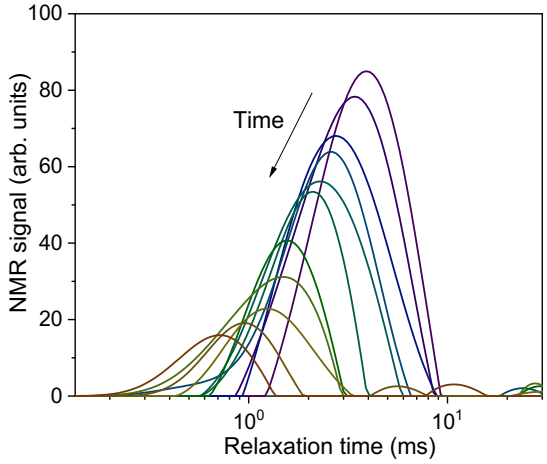

Figure 3: Distribution of NMR relaxation at different times (every two hours) during a drying test of a 0.8 cm thick sample with $\delta = 6\,\mathrm{cm}$.

Let us now look at the drying of the cellulose packing as it appears from MRI profiles at successive times (see Figure 4). Before focusing on the main trends of the drying behavior, we mention two artefacts. We can observe some apparent shift of the (right) base of the first profiles towards the left, as if some dry region was developing in the top layers of the sample. However, we finally observed some shrinkage, say of about 2 mm, at the end of the test, which suggests that the initial progressive shift is associated with this shrinkage and no significant dry front developed. We can also observe that the bound water distribution, as it appears from the initial profiles, is not perfectly homogeneous (i.e. the MRI signal is not flat in Figure 4): there is more bound water in the central part of the sample. For the other experiment presented here the profiles were also slightly non uniform, but in that case the largest saturation point was observed at the approach of the sample bottom. This is likely due to some heterogeneity of the cellulose concentration in the initial packing. We stress that the impact of these artefacts on the main trends is minor. Finally the relative uncertainty associated with this effect is about 5%.

The main trends show that the extraction of bound water from a cellulose packing has nothing to do with the typical drying under similar air flux conditions of simple porous materials initially filled with free water [42]. In that case capillary effects are dominant, leading to a homogeneous desaturation during a long first period. On the contrary, here, a strong gradient of water content develops immediately in the water distribution and spreads in the sample from the top to the bottom; note that these heterogeneities are much stronger than the initial one (see above); when this gradient has reached the sample bottom, the profiles become progressively flatter.

These features are characteristics of a diffusion process. At this stage one could consider that the water diffuses longitudinally in the form of bound water through the solid structure, similarly to what happens in wood [40]. However, here, considering the large sample porosity, another scenario could happen where water vapor plays a significant role. In the following, we will quantify and compare both contributions, i.e. bound water and vapor diffusions, in order to identify the right scenario.

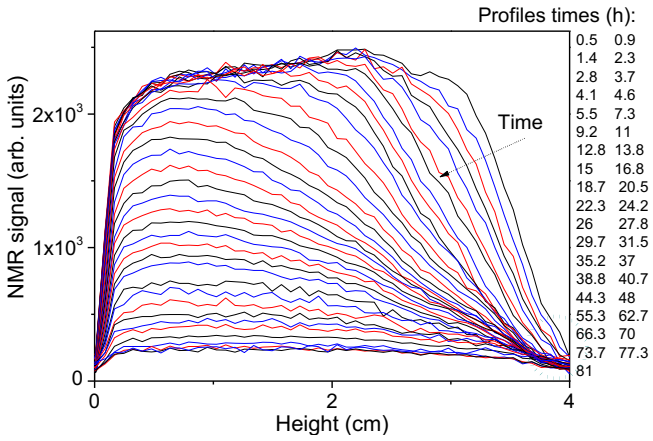

Figure 4: Drying of a 4 cm cellulose sample. The dry air flux is along the sample top (right side). Successive bound water distributions in time as obtained by averaging basic profiles over successive periods (see corresponding times in caption) of progressively increasing durations. The dotted circle indicates the region of probable shrinkage.

IV. A SIMPLE MODEL FOR BOUND WATER TRANSPORT IN TEXTILE

A. Transport by coupled vapor-bound water diffusion

We consider a porous medium of porosity ε, made of a solid structure, which can absorb water in the form of bound water (see Figure 5). We look at the water transport properties in one direction only, i.e. x. The material properties are assumed to be homogeneous in planes perpendicular to x axis. Thus, the evolution of averaged variables over cross-sections fully describes the process. We neglect porosity or sample volume changes resulting from bound water content variations. In this context, the water transport is fully described by the distribution of moisture content at each time t, $s(x,t)$, i.e. the bound water to (dry) cellulose mass ratio, and the distribution of relative humidity in the pores, $n(x,t)$. Here we basically consider moisture transport induced by a change in the boundary conditions with respect to some previous equilibrium under ambient temperature. We will only consider temperature distribution changes and heat transfers in the medium as an effect of moisture transfers.

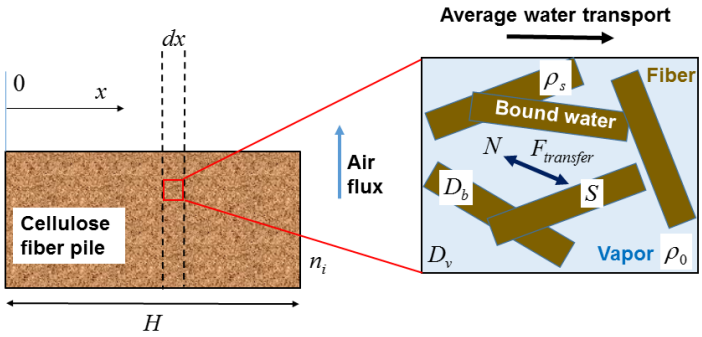

Figure 5: Scheme of the internal structure of the cellulose fiber pile and main variables.

The variations of s and n may be looked at in their respective media (i.e. solid and void networks) and be described by diffusion equations, taking into account the transfer of water between the two networks, expressed in the form of a local flux $F_{transfer}$. We first describe the conservation of mass for each water type, considering N the mass of vapor molecules, and S the mass of bound water molecules, per unit length of cross-sectional layer:

$$\frac{\partial N}{\partial t} = D_v \frac{\partial^2 N}{\partial x^2} - F_{transfer} \qquad (2a)$$

$$\frac{\partial S}{\partial t} = D_b \frac{\partial^2 S}{\partial x^2} + F_{transfer} \qquad (2b)$$

in which D_v is the diffusion coefficient of vapor through the void network, and D_b the diffusion coefficient of bound water through the solid network. As long as the pore size is much larger than the mean free path of water molecules D_v may be written as $D_v \approx \varepsilon D_0/\tau$ [43], with $D_0 = 2.7\times10^{-5}\ \mathrm{m^2\ s^{-1}}$ the diffusion coefficient of vapor in air and τ the tortuosity of the (void) medium, and similarly $D_b = (1-\varepsilon)D_L/\tau'$, with τ'

the tortuosity of the (solid) medium, and D_L the diffusion coefficient of bound water along the fiber.

Eliminating $F_{transfer}$ from (2a) and (2b) we get

$$\frac{\partial N}{\partial t}+\frac{\partial S}{\partial t}=D_v\frac{\partial^2 N}{\partial x^2}+D_b\frac{\partial^2 S}{\partial x^2} \qquad (3)$$

N and S are obviously related to n and s. We can write $N=n\rho_0\Omega_p$ in which Ω_p is the pore volume per unit length and $\rho_0=0.02\,\mathrm{kg\,m^{-3}}$ the saturation vapor density at our ambient temperature (22.5°C). We also have $S=s\rho_s\Omega_s$, in which Ω_s and ρ_s are the volume and density of the dry solid phase. Using the sample volume Ω and the porosity we get $S=s\rho_s(1-\varepsilon)\Omega$ and $N=n\rho_0\varepsilon\Omega$.

In the absence of exchanges between the bound water and the vapor, the vapor would be rapidly transported so as to reach equilibrium with the conditions imposed outside. In parallel the bound water could diffuse through the solid structure, but would not evaporate even along the sample surface. After some time this leads to a neutralization of the transport. As a consequence, drying occurs only if there is a continuous exchange between bound water and vapor, which induces a vapor transport inside the sample depending on bound water – vapor exchanges. These exchanges govern the relation between the local moisture content in the structure and the relative humidity in the surrounding air. Ideally, the knowledge of the relationship between n and s would allow to solve equation (3). From a general point of view we can search for the dependence of s as a function of the history of n, i.e. the sorption dynamics.

Actually, this question of the sorption dynamics, which plays a critical role in the model, is central also in the models developed during the past 80 years. Those models assume that absorption is not instantaneous. This was initially suggested by Nordon and David [26-27], relying on some observations of sorption kinetics in a single wool fiber with a "vibroscope" [44-46]. However, in these experiments, the characteristic time for the main absorption (say, 80 to 90% of the final amount) is typically less than one minute when the dry fiber is placed in contact with wet air at 80 or 90% RH. Such a time is actually much smaller than the typical time for water transport under real conditions, i.e. typically a few hours for the drying of a centimetric cellulose sample under a fast dry air flow. This means that over such duration we are certainly close to equilibrium at any time in the structure, i.e. the remaining difference is negligible.

Let us quantify this process. Water vapor molecules first hit the fiber walls then diffuse through the structure. The exchange between vapor and fiber walls being fast, the equilibrium assumption is valid if the diffusion of bound water through the thickness of the fibers is sufficiently fast compared to the typical duration (Δt) of the transport experiment. This is so if the characteristic time of penetration by diffusion is much smaller than Δt, i.e. if $e^2/D_T \ll \Delta t$, in which e is the fiber radius and D_T the diffusion coefficient of bound water in the solid structure in the direction perpendicular to the wall surface. Using for D_T the order of magnitude for D_L as found in [47] from molecular simulations for amorphous cellulose, i.e. $10^{-10}\,\mathrm{m^2\,s^{-1}}$, we find a characteristic time of diffusion of the order of 1 s. Even if for our material made of crystals in an amorphous matrix D_T is likely somewhat smaller, this order of magnitude shows that over the typical duration of our tests (i.e. Δt > 10000 s) the equilibrium is largely reached.

As a consequence, here we consider that locally, at any time, we are close to the equilibrium between the relative humidity and the bound water content, which implies that $s=f(n)$, in which f is the sorption or desorption curve, depending on whether n is increasing or decreasing. Note that for our material f is the common sorption and desorption curve (see Figure 1).

Taking into account this result we deduce that n and s are in the same order, and this conclusion also applies to their spatial or time variations. Since $S/N=(s/n)(\rho_s/\rho_0)((1-\varepsilon)/\varepsilon)$ is in general much larger than 1 since $\rho_0/\rho_s \ll 1$, we deduce that we can neglect $\partial N/\partial t$ compared to $\partial S/\partial t$ in equation (3).

Equation (3) finally writes

$$\frac{\partial s}{\partial t}=D\frac{\partial^2 f^{-1}(s)}{\partial x^2}+D_b\frac{\partial^2 s}{\partial x^2} \qquad (4)$$

with $D=\dfrac{\rho_0}{\rho_s}\dfrac{\varepsilon^2}{(1-\varepsilon)\tau}D_0$

Knowing the exact expression for the sorption curve $f(s)$, the equation (4) will be solved numerically for initial and boundary conditions corresponding to our experiments. Let us for example consider the simplest case of a linear sorption or desorption curve, i.e.

$f(n) = \alpha n$: equation (4) is a simple diffusion equation with a diffusion coefficient $D/\alpha + D_b$. In this simplified context we see that the transport of humidity through a hygroscopic porous medium is essentially described by a simple diffusion process with a diffusion coefficient depending on the vapor diffusion, vapor – bound water exchange, and bound water diffusion.

By comparing the orders of magnitude of D/α and D_b we can also identify the leading diffusion process: For a cellulosic solid phase (i.e. with a density $\rho_s \approx 1500\ \mathrm{kg\,m^{-3}}$ and $\alpha \approx 0.2$), a porosity of 80% and a tortuosity equal to 1.3 (see Appendix 2), D/α is in the order of $4\times10^{-9}\ \mathrm{m^2\,s}$. This is much larger than the value of the diffusion coefficient of bound water through the cellulose structure (estimated for $n = 1$), i.e. $D_b = (1-\varepsilon)D_L/\tau'$, which is significantly smaller than $10^{-10}\ \mathrm{m^2\,s}$ according to the value found from simulations for D_L [47] and the values for the porosity and the tortuosity of the solid structure, the latter likely being significantly larger than 1. This indicates that the absorbed water is transported through the structure, thanks to vapor, where it may then be stored or extracted (i.e. $\partial s/\partial t > 0$ or < 0), depending on the boundary and initial conditions, and we can neglect the second term in the right hand-side of (4).

B. Convective drying of cellulose

Equation (4) may be solved as soon as the boundary conditions are properly defined. In the following we determine these boundary conditions in the case of a simple air flux along the free surface of the sample.

We consider the case of a porous material, subjected along its surface to a given air flux, while the other external surfaces of the sample are not permeable. Since the air flux can hardly penetrate the sample which is a finely divided dead end network, the air essentially flows along this surface.

Let us now consider more precisely that the RH of the air is n_0, and that it flows along a plane maintained at a RH n_i. The plane is sufficiently long so that edge effects can be neglected. Assuming a uniform tangential velocity V, the vapor distribution is described by an advection-diffusion equation, whose solution in steady-state expresses as $n_i + (n_0 - n_i)\mathrm{erf}(x/2\sqrt{D_0 y/V})$, in which x is here the distance from the surface and y the position along the surface starting at $y = 0$. As a consequence, for a given position y the local vapor flux in the direction normal to the surface writes $J_0 = -\rho_0 D_0(\partial n/\partial x) = \rho_0 D_0 (n_i - n_0)/d$, with $d = \sqrt{\pi D_0 y/V}$. We deduce that the total vapor flux, i.e. the drying rate, found by integrating this flux over the surface, may be written in a similar way [48], with now $\partial n/\partial x = (n_i - n_0)/\delta$, with $\delta = <1/d>$. Extrapolating this result to more complex air flows and a surfaces of any shape we deduce that the vapor flux can be expressed in the same way, with δ depending on the area of the surface, its shape, size and roughness, and more critically on the upstream air flux characteristics.

As drying affects the water content in the porous material n_i will evolve in time, but the characteristic distance δ, whose value is independent on the internal material properties, does not change. As a consequence δ may be estimated from the initial drying rate of the sample under given initial conditions s_i: indeed, in that case, in the context of our model with the assumption of local equilibrium between n and s, n is equal to $n_i(s_i)$ all along the free surface of the sample (i.e. including void and solid regions).

Finally, in contrast with simple porous media filled with water for which capillary effects play the major role, here the current drying rate depends on the mechanism of bound water and vapor transport in the whole medium, leading to the current value of n_i associated with the value of s_i. The solution of this problem is found by solving numerically equation (4) with the initial conditions on s and the boundary condition for the mass flux of water at the top surface J_0 and no mass flux through the bottom surface. The details of these numerical simulations are given in Appendix 2.

C. Comparison with experiments

Mass vs time curves

Let us start by analyzing the mass variations of the whole sample as a function of time. In order to compare more directly the different results the water mass vs time curves are drawn in the form of the saturation as

a function of time (see Figure 6). Here the saturation means the ratio of the current water mass to the initial one (let us recall that all the samples are initially almost or fully saturated). The saturation is also the ration of the current to the initial moisture content. Obviously we observe that the drying takes a longer time for thicker samples, i.e. larger H values, and for lower air flux, i.e. larger δ values (see Figure 6).

We can then compare the predictions of the model with these data. It appears that the model perfectly predicts the results, except in some cases at the end of the process, i.e. for a saturation below 10% (see Figure 6). This excellent prediction of the data is obtained over a range of thicknesses between 0.5 and 4 cm, and for different air flux intensities leading to δ ranging from 4 mm to 6 cm.

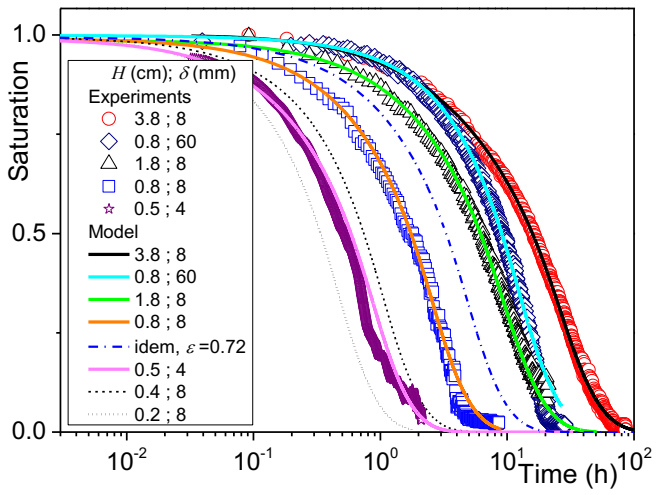

Figure 6: Saturation vs time curve for drying tests under different conditions, i.e. different sample thicknesses (H) and drying rates (described through the parameter δ, see text). Except when mentioned experimental and simulation data are for a porosity (ε) of 0.82.

Saturation profiles along sample depth

We now look in more details at the model predictions concerning the spatial distribution of bound water in time. For the sake of clarity we concentrate on a limited series of MRI profiles among the large number obtained. For each experiment we rescale the profiles by the initial one, which makes it possible to get a constant plateau in the saturated region (see Figures 5-6). Actually, this is a rough approach to disregard the effect of the previously mentioned slight concentration heterogeneity (maximum saturation level difference of 10%), without taking into account its detailed impact on the transport phenomena during the process. In this way, we look at the distribution in time of the local saturation, defined as the ratio of the local current moisture content to the initial one.

The model successfully predicts the measured diffusion process (see Figures 7-8): first a front penetration, then a progressive decrease of the saturation with a slight gradient. The quantitative agreement between the model predictions of bound water distributions in time is remarkable for the test with the 1.8 cm sample (see Figure 7). A slight discrepancy is just observed in the second part of the process, say around ten hours. For the test with the 3.8 cm sample (see Figure 8) an excellent agreement is observed at the beginning, i.e. during the front penetration, and at the end, when the saturation is almost homogeneous; there appears some discrepancy of the theoretical and experimental distribution shapes in the intermediate range, say between 12 and 25 hours. However, we can remark that the distributions in this range have similar shapes but seem to be slightly deformed in the two directions, which suggests that this discrepancy is due to the sample shrinkage, a phenomenon which is negligible (smaller than 1 mm) for the 1.8 cm sample.

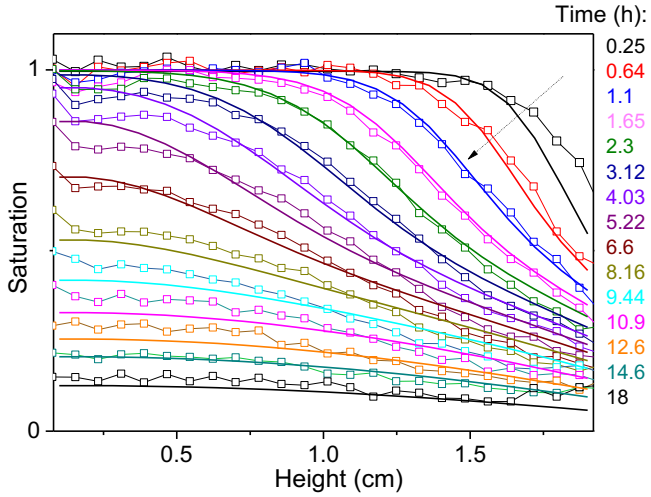

Figure 7: Drying test with 1.8 cm sample ($\delta = 8$ mm). Saturation profile measured by MRI (symbols) at different times (indicated in caption), and model predictions (corresponding continuous curves) for the same times.

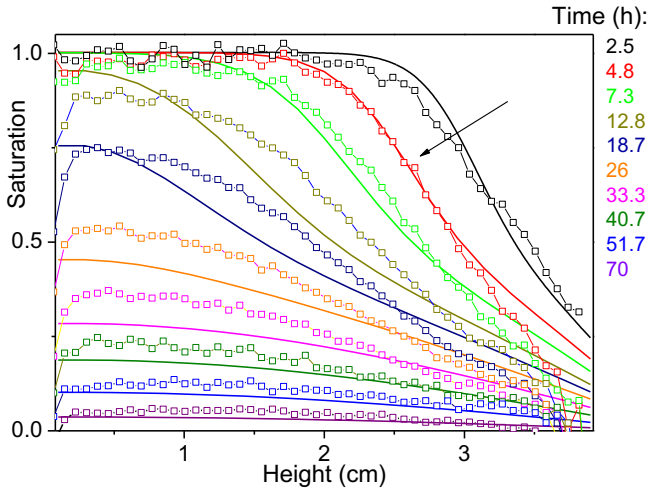

Figure 8: Drying test with 3.8 cm sample ($\delta = 8$ mm). Saturation profile measured by MRI (symbols) at different times (indicated in caption), and model predictions (corresponding continuous curves) for the same times.

D. Characteristic times of drying or humidification of textile

Without fitting any parameter, our model predicts very well the mass vs time curves under different conditions (sample thickness and drying rate) within wide ranges. It also predicts very well the saturation evolution in time at the local scale. Under such conditions we can be fully confident about the validity of physical assumptions underlying this model, mainly the sorption equilibrium at each time.

Note that the solid textile bulk density and tortuosity probably vary marginally from one material to another, so they may be considered as constant in the model. Also, we could see through various simulations that the exact shape of the sorption curve plays a relatively minor role on the drying curve, the total duration of drying being mostly governed by the maximum moisture content at 100% RH, which is equal to α in the linear case. In contrast, the sample thickness plays a major role on the drying, as it can be appreciated in Figure 6. At last the sample porosity also plays an important role (see Figure 6) as the diffusion coefficient is proportional to the squared porosity. In particular, all other parameters being constant (with values of this study), in the extreme case when ε decreases below 0.2, D/α can become in the order or smaller than D_b. This means that bound water diffusion starts to play a significant role in the water transport in dense fabrics.

This model does not specifically apply to drying, it may also be used to predict the evolution of the bound water content in a textile sample for any initial bound water content and any history of RH along the boundaries, by solving the equation (4). Detailed predictions of the characteristic times of change of the bound water content under specific conditions can thus be done.

A complete overview of the model predictions can be obtained in the case of a linear sorption curve (or approximate representation of the sorption curve by a straight line), which also provides good estimations in other cases. Indeed, in that case equation (4) has an analytical solution (see Appendix 3) from which we can plot the total saturation as a function of the dimensionless time $Dt/\alpha H^2$ for different values of the parameter $L = \tau H/\varepsilon^2\delta$ (see Figure 10). For a given air flux L increases with the sample thickness, the tortuosity of the structure, and decreases when the porosity increases. For given material properties it also decreases when the air flux intensity decreases, i.e. when δ increases. This parameter finally expresses the "difficulty" of drying the material under these conditions, through the product of some characteristic length to dry, i.e. $\tau H/\varepsilon^2$, and the air flux intensity, expressed through $1/\delta$.

Two drying regimes appear (see Appendix 3). For sufficient low L values (i.e. $L < 1$) the model predicts almost uniform saturation profiles in time (see Figure 11) and a drying rate simply imposed by the external air flux: the drying rate slowly decreases, proportionally to the saturation which imposes (due to the sorption equilibrium) the value of the vapor density n_i along the free surface, which is also the current uniform value in the sample. Smaller L values induce lower constant drying rate (see Figure 10).

For large values of L significant heterogeneity in the saturation distribution develops (see Figure 11), and the drying rate becomes independent of the air flux for sufficiently large L, i.e. $L >> 1$ (see Figure 11). Note that for our tests L ranges from 0.23 to 8, so that we almost cover all regimes.

From this model it is also possible to get relevant generic estimation of the dimensionless characteristic time of the process ($T = Dt/\alpha H^2$). We define this time as the one for which the average saturation reaches one third. It appears to be equal to about $1/L$ when $L < 1$, and 0.36 when $L >> 1$ (see inset of Figure 10). This gives:

$$L<1 \Rightarrow T=\alpha(1-\varepsilon)\rho_s \delta H/\rho_0 D_0 \quad (5)$$

$$L>>1 \Rightarrow T=0.36\alpha(1-\varepsilon)\rho_s \tau H^2/\rho_0 \varepsilon^2 D_0 \quad (6)$$

Since the equations of the model are the same if we replace s by $\alpha - s$, we get the same solution, now for $\alpha - s$ if the boundary and initial conditions are also changed to $\alpha - s$ values. This change corresponds to a sample initially dry ($s=0$) which is suddenly placed in contact with a saturated air flux ($n=1$) characterized by a parameter δ, and we assume no exchange through the sample bottom ($x=0$). Then the characteristic time for humidification of the textile sample is found from equations (5) and (6) depending on the value of L. This provides the typical time during which a clothes initially dry will protect the body against ambient humidity, or the characteristic time before a mask will be completely wet.

V. CONCLUDING REMARKS

For the first time here we were able to present a full set of data showing the spatial distribution of bound water in a model textile during drying. A simple model assuming sorption equilibrium at any time is able to almost perfectly predict the observations without any fitting parameter, the largest uncertainty being on the air flux characteristics and its impact on the drying rate. Also some shrinkage may slightly affect the predictions.

Comparisons with empirical models are difficult as they generally concern materials for which we do not have the characteristics used in our model, such as the porosity and the thickness, and the information on the air flux is not sufficient. Comparisons with complete models (derived from [18]) would be possible. Actually, the equation of vapor transport (water mass conservation) is similar to ours if a similar value for the diffusion coefficient for vapor through the structure (D_v) is used and if the sorption dynamics is supposed to be instantaneous (with respect to the characteristics time of the test). However, these models have not been developed up to the point of providing the practical predictions concerning the characteristic times of humidification or drying as we propose in this paper. An interesting point would be to study, within the frame of our approach, the impact of the sorption dynamics on this characteristic time. This would for example be useful to deal with thicker fibers such as those used for fiberboard in construction. However, this represents a significant work which is left for the future.

Our results in particular validate the initial assumption of Henry [18] on the sorption equilibrium in most practical cases, which constitutes a critical result which will greatly facilitate the modelling of such systems. Also, it is likely that this result can be used for the predictions of thermal transfers, and will facilitate the hygrothermal modelling approaches. Water desorption is indeed associated with a latent heat comparable to that of evaporation from standard liquid state. Thus, we expect significant heat transfer resulting from the bound water extraction from the sample. However, since for all our experiments the process is rather slow and the amount of bound water to evaporate rather small, the temperature is certainly maintained around the ambient one thanks to the air flux, to which heat is transferred. Under these conditions, there is no impact of heat transfer on the mass transfer.

The situation would be different for faster processes, which would induce local temperature changes, possibly affecting the desorption curve, the vapor diffusion coefficient and the saturation vapor density. Note that as long as the air flux is at the same temperature as the sample (at least initially), a drastically faster drying is likely necessary to have such coupling between heat transfers and moisture transport. Coupling will be more easily observed with a hot air flux. The problematic is analogous for mechanical effects: they may have an impact for sufficiently thick samples or fast processes.

At last, we have seen that the model can be used for straightforward analytical predictions of the humidification or drying characteristics of textile materials. In particular one can predict the typical time of humidification of a mask submitted to a 100% air flux (considering that most of the air flux is finally tangential to the surface due to side leakage [49-50]).

Acknowledgements

We gratefully acknowledge funding from the Labex MMCD provided by the national program Investments for the Future of the French National Research Agency (ANR-11-LABX-022).

The present address of Xiaoyan Ma is: Beihang Hangzhou Innovation Institute, Yuhang, Hangzhou, China.

APPENDIX 1: DRYING CURVES: COMPARISON BETWEEN MRI AND WEIGHING DATA

Here we present data for the saturation vs time as deduced by integration of the NMR signal in the profiles

obtained by MRI, and we compare with data obtained by weighing the sample during an experiment outside the magnet but under similar air flux conditions. There is more scatter in the latter data due to the variation in the interaction between the air flux and the sample, but the two set of data are very close (see Figure 9).

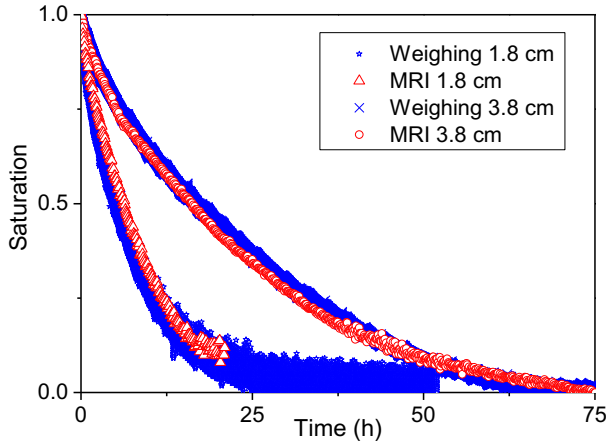

Figure 9: Comparison between MRI data and weighing for two tests with different thicknesses ($\delta = 8\ \mathrm{mm}$ in both cases).

APPENDIX 2: NUMERICAL SIMULATIONS

We adopt the Finite Differential Method (FDM) to solve the partial differential equation, with specific initial condition and boundary conditions. The method consists in converting the differential equation (governing equation) and its boundary conditions to a system of linear equations expressed in a discrete way. Such a system is then solved by matrix algebra approach. The explicit method is adopted, which is a forward difference for time and a second-order central difference for the space derivative. Adaptive time stepping is used to ensure the stability condition.

Dealing with the drying process, the initial humidity is considered homogeneous at 100%. The left boundary (distance $x = 0$), corresponding to the impermeable bottom surface, is set as no-flux boundary condition, and the right boundary (free surface, i.e. $x \geq H$) is Fourier-type (convectional boundary), i.e., the relative humidity value along the interface n_{i} changes progressively to the ambient condition ($n_0 = 0$) along the characteristic distance of δ.

The distributions of relative humidity $n(x,t)$ are obtained first, then converted to the distribution of moisture content at each time point $s(x,t)$ according to the desorption isotherm curve.

For these simulations the fixed parameters are: the saturation vapor density at 22.5°C $\rho_0 = 0.02\ \mathrm{kg\,m^{-3}}$, $\rho_s \approx 1500\ \mathrm{kg\,m^{-3}}$ the density of the dry solid phase, $D_0 = 2.7\times10^{-5}\ \mathrm{m^2\ s^{-1}}$ the diffusion coefficient of vapor in air, the porosity $\varepsilon = 0.82$, the tortuosity $\tau = 1.2$. This value of tortuosity is taken from an extensive review of experimental and theoretical data for fiber tortuosity [51]. The only two parameters changing from one test to another are the sample thickness H, which is measured and assumed constant during the test, and the characteristic thickness of vapor diffusion resulting from air flux δ, which is estimated from the slope of the mass vs time curve in the very first time of drying. The uncertainty on this value is about 15%.

APPENDIX 3: ANALYTICAL SOLUTION OF THE MODEL FOR A LINEAR SOPRTION CURVE: $s = \alpha n$

In that case in the porous medium the flux of s writes $(D/\alpha)\nabla s$ which corresponds to a mass flux $J = \rho_s(1-\varepsilon)D(\partial s/\partial x)/\alpha$, which is equal to J_0 at the interface, which gives $\rho_s(1-\varepsilon)D(\partial s/\partial x)/\alpha = \rho_0 D_0\, n_i/\delta = \rho_0 D_0\, s_i/\alpha\delta$ (for $n_0 = 0$). We deduce that the condition along the free surface may be written as

$$(D/\alpha)\nabla s = \beta s_i \qquad (7)$$

with $\beta = \dfrac{\rho_0 D_0}{\alpha\rho_s(1-\varepsilon)\delta}$. The solution of equation (4) for $s = \alpha n$, namely $\partial s/\partial t = (D/\alpha)\partial^2 s/\partial x^2$, with the boundary condition (7) for $x = H$, and $(\partial s/\partial x) = 0$ for $x = 0$ (i.e. no flux through the sample bottom) is given [52] as follows. The local saturation writes $\psi = s/s_0$, with s_0 the moisture content at initial time. The saturation profile at any time expresses as

$$\psi(x,t) = \sum_{p=1}^{\infty} \frac{2L\cos(\beta_n x/H)\exp\left(-\beta_n{}^2 Dt/H^2\right)}{(\beta_n{}^2 + L^2 + L)\cos\beta_n} \qquad (8)$$

in which $L = \alpha\beta H/D = \dfrac{\tau H}{\delta\varepsilon^2}$ and β_n are the positive solutions of $\beta_n \tan\beta_n = L$.

The average bound water saturation over the sample thickness (i.e. $\Psi = <\psi>$) expresses as:

$$\Psi = 1 - \sum_{p=1}^{\infty} \frac{2L^2\exp\left(-\beta_n{}^2 Dt/H^2\right)}{(\beta_n{}^2 + L^2 + L)\beta_n{}^2} \qquad (9)$$

Two regimes may be distinguished. For sufficient low L values (i.e. $L<<1$) the successive profiles are essentially horizontal (see Figure 11): the saturation decreases homogeneously in time. In that case the RH, at equilibrium with the bound water content, is also almost uniform in the sample so that the saturation determines the drying rate, through the value of $n_i = s_i/\alpha$. Thus, the drying rate continuously decreases as the saturation decreases. Furthermore, the drying rate is simply proportional to $1/\delta$ and thus to L (see Figure 10).

For sufficiently large L values (i.e. $L>>1$) the profiles are strongly curved at the approach the top surface of the sample from the very beginning (Figure 11). In that case the drying rate rapidly decreases at the beginning of the test and, as we increase L, the drying curves represented as a function of the dimensionless time $\sqrt{Dt/\alpha H^2}$ tend to an asymptotic curve (see Figure 10).

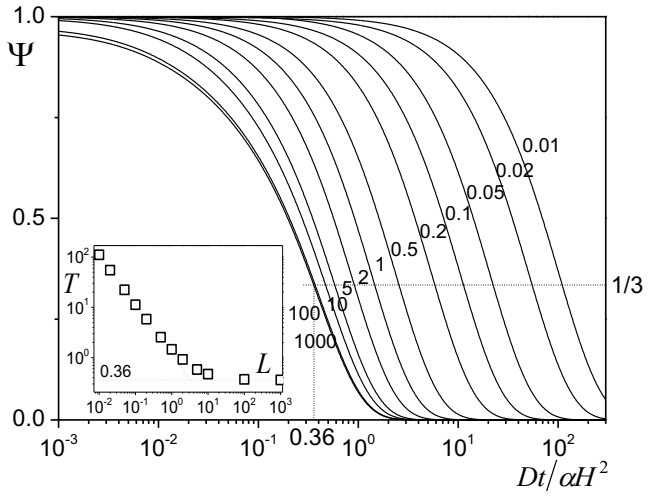

Figure 10: Drying curves predicted from the model (equation (9)), in terms of average saturation as a function of dimensionless time, for different L values indicated in the graph. The inset shows the dimensionless time value, i.e. $T = Dt/\alpha H^2$, for which the saturation reaches 1/3, as a function of L. In this inset the inclined dotted line has a slope -1.

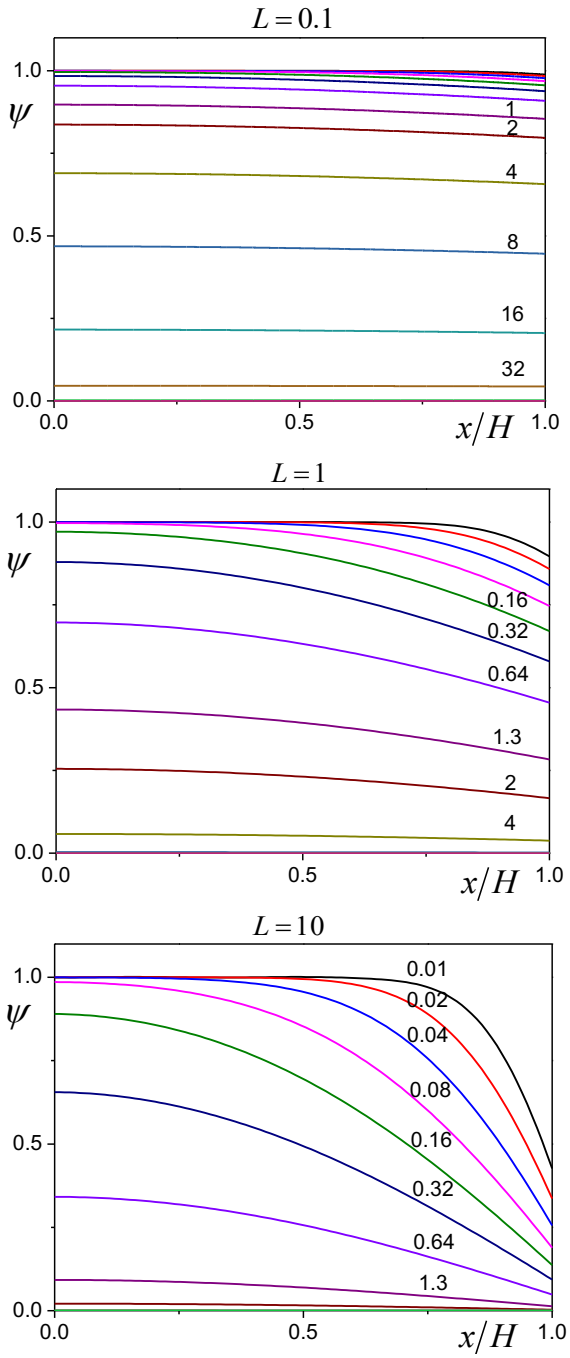

Figure 11: Bound water distribution in time as a function of the dimensionless distance from bottom (sample top at $x = H$) as predicted by the model for different values of L. In each case the distributions are drawn for the same series of dimensionless times ($Dt/\alpha H^2$) (same line color for same dimensionless time), some of them being indicated in the graphs.

References

[1] J.C. Barnes, B.V. Holcombe, Moisture sorption and transport in clothing during wear, Textile Res. J., 66, 777-786 (1996)

[2] T. Fukazawa, G. Havenith, Differences in comfort perception in relation to local and whole body skin wettedness. Eur. J. Appl. Physiol. 106, 15–24 (2009)

[3] N. Gerrett, B. Redortier, T. Voelcker, G. Havenith, A Comparison of Galvanic Skin Conductance and Skin Wettedness as Indicators of Thermal Discomfort during Moderate and High Metabolic Rates, J. Thermal Biology, 38, 530-538 (2013)

[4] M. Raccuglia, B. Sales, C. Heyde, G. Havenith, S. Hodder, Clothing comfort during physical exercise – Determining the critical factors, Applied Ergonomics, 73, 33-41 (2018)

[5] G. Havenith, M.G. Richards, X. Wang, P. Bröde, V. Candas, E. den Hartog, I. Holmer, K. Kuklan, H. Meinander, W. Nocker, Apparent latent heat of evaporation from clothing: attenuation and ''heat pipe'' effects**,** J. Applied Physiology, 104, 142-149 (2008)

[6] M. Jerman, I. Palomar, V. Koci, R. Cerny, Thermal and hygric properties of biomaterials suitable for interior thermal insulation systems in historical and traditional buildings, Buidling and Environment, 154, 81-88 (2019)

[7] M. Jerman, R. Cerny, Effect of moisture content on heat and moisture transport and storage properties of thermal insulation materials, Energy and Buildings, 53, 39-46 (2012)

[8] D.R. O'Dell, W.W. Carr, Effect of humidity on the drying rates of carpet tiles, Textile Research Journal, 66, 366-376 (1996)

[9] J.M. Courtney, A. Bax, Hydrating the respiratory tract: An alternative explanation why masks lower severity of COVID-19 disease, Biophysical Journal, 16, 994-1000 (2021)

[10] C.D. Zangmeister, J.G. Radney, M.E. Staymates, E.P. Vicenzi and J.L. Weaver, Hydration of Hydrophilic Cloth Facial Coverings Greatly Increases the Filtration Properties for Nanometer and Micron-sized Particles, *ACS Applied Nano Materials.* 4, 2694–2701 (2021)

[11] U. Akyol, K. Kahveci, A. Cihan, Determination of optimum operating conditions and simulation of drying in a textile drying process, The Journal of The Textile Institute, 104, 170-177 (2013)

[12] K.C. Parsons, G. Havenith, I. Holmer, H. Nilsson, J. Malchaire, The effects of wind and human movement on the heat and vapour transfer properties of clothing, Ann. Occup. Hyg., 43, 347-352 (1999)

[13] B. Farnworth, A numerical model of the combined diffusion of heat and water vapor through clothing, Textile Research Journal, 56, 653-665 (1986)

[14] G. Havenith, I. Holmer, E.A. den Hartog, K.C. Parsons, Clothing evaporative heat resistance – Proposal for improved representation in standards and models, Ann. Occup. Hyg., 43, 339-346 (1999)

[15] S.R. Liu, X.-Q. Dai, Y. Hong, Prediction of the water evaporation rate of wet textile materials in a pre-defined environment, Int. J. Clothing Science and Technology, 32, 356-365 (2020)

[16] S. Ulku, D. Balkose, T. Caga, F. Ozkan, S. Ulutan, A study of adsorption of water vapour on wool under static and dynamics conditions, Adsoprtion, 4, 63-73 (1998)

[17] S. Lee, S.K. Obendorf, Statistical modeling of water vapor transport through woven fabrics, Textile Research Journal, 82, 211-219 (2012)

[18] P.S.H. Henry, Diffusion in absorbing media, Proc. Roy. Soc. London A, 171, 215-241 (1939)

[19] Nordon, P., B.H. Mackay, J.G. Downes, and G.B. Mc Mahon, "Sorption Kinetics of Diffusion Coefficients and Analysis of Integral Sorption," *Textile Res. J.*, **40**, 461–469 (1970)

[20] H.E. Daniels, Propagation of temperature changes through textiles in humid atmospheres. Part IV. Extended theory temperature propagation through textiles, Trans. Faraday Soc., 37, 506-517 (1941)

[21] Y. Li, Q. Zhu, K.W. Yeung, Influence of thickness and porosity on coupled heat and liquid moisture transfer in porous textiles, Textile Res. J., 72, 435-446 (2002)

[22] Y. Li, Q. Zhu, Simultaneous heat and moisture transfer with moisture sorption, condensation, and capillary liquid diffusion in porous textiles, Textile Res. J., 73, 515-524 (2003)

[23] Y. Li, B.V. Holcombe, A two-stage sorption model of the coupled diffusion of moisture and heat in woll fabrics, Textile Res. J., 62, 211-217 (1992)

[24] Y. Li, Z. Luo, An improved mathematical simulation of the coupled diffusion of moisture and heat in wool fabric, Textile Res. J., 69, 760-768 (1999)

[25] Q. Zhang, B. Li, W. Sun, Heat and sweat transport through clothing assemblies with phase changes, condensation/evaporation and absorption, Proc. Roy. Soc. A, 467, 3469-3489 (2011)

[26] P. Nordon, H.G. David, Coupled diffusion of moisture and heat in hygroscopic textile materials, Int. J. Heat Mass Transfer, 10, 853-866 (1967)

[27] H.G. David, P. Nordon, Case studies of coupled heat and moisture diffusion in wool beds, Textile Res. J., 39, 166-172 (1969)

[28] M. Woloszyn, C. Rode, Tools for performance simulation of heat, air and moisture conditions of whole buildings, Building Simulation, 1, 5–24 (2008)

[29] J. Delgado, N. M. Ramos, E. Barreira, V. De Freitas, A critical review of hygrothermal models used in porous building materials, Journal of Porous Media 13, 221-234 (2010)

[30] S. Dubois, A. Evrard, F. Lebeau, Modeling the hygrothermal behavior of biobased construction materials, *J. Building Phys*., 38, 191-213 (2013)

[31] T. Busser, J. Berger, A. Piot, M. Pailha, M. Woloszyn, Comparison of model numerical predictions of heat and moisture transfer in porous media with experimental observations at material and wall scales: An analysis of recent trends, *Drying Technology*, 37, 1363-1395 (2019)

[32] T. Busser, J. Berger, A. Piot, M. Pailha, M. Woloszyn. Comparative Study of Three Models for Moisture Transfer in Hygroscopic Materials, *Transport in Porous Media*, 126, 379–410 (2019)

[33] N. Bhouri, Thermodynamical and dimensional behavior of textile materials submitted to climatic variations, PhD thesis, Univ. Nancy (2009) (in French)

[34] M. Chen, B. Coasne, R. Guyer, D. Derome, J. Carmeliet, Role of hydrogen bonding in hysteresis observed in sorption-induced swelling of soft nanoporous polymers, Nature Communications, 9, 3507 (2018)

[35] N. Ben Abdelouahab, A. Gossard, X. Ma, H. Dialla, B. Maillet, S. Rodts, P. Coussot, Understanding mechanisms of drying of a cellulose slurry by magnetic resonance imaging, Cellulose, 28, 5321-5334 (2021)

[36] P.T. Callaghan PT, *Principles of Nuclear Magnetic Resonance Microscopy*, Clarendon, Oxford (1993)

[37] K.P. Whittall, A.L. MacKay, Quantitative interpretation of NMR relaxation data, J. Magn. Reson. 84, 134–152 (1989)

[38] S.W. Provencher, A constrained regularization method for inverting data represented by linear algebraic or integral equations, Comput. Phys. Commun., 27, 213–227 (1982)

[39] P. Faure, S. Rodts, Proton NMR relaxation as a probe for setting cement pastes, Magn. Reson. Imaging, 26, 1183–1196 (2008)

[40] H. Penvern, M. Zhou, B. Maillet, D. Courtier-Murias, M. Scheel, J. Perrin, T. Weitkamp, S. Bardet, S. Caré, P. Coussot, How bound water regulates wood drying, Physical Review Applied, 14, 054051 (2021) https://doi.org/10.1103/PhysRevApplied.14.054051

[41] M. Zhou, S. Caré, D. Courtier-Murias, P. Faure, S. Rodts, P. Coussot, Magnetic resonance imaging evidences of the impact of water sorption on hardwood capillary imbibition dynamics, *Wood Science and Technology*, **52**, 929-955 (2018)

[42] J. Thiery, S. Rodts, D.A. Weitz, P. Coussot, Drying regimes in homogeneous porous media from macro- to nanoscale, Phys Rev Fluids, 2, 074201 (2017). https://doi.org/10.1103/PhysRevFluids.2.074201

[43] J.F. Daian, *Equilibrium and transfer in porous media 1 – Equilibrium states*, Wiley, New York, 2014

[44] J.G. Downes, B.H. Mackay, Soprtion kinetics of water vapor in wool fibers, J. polymer Science, 28, 45-67 (1958)

[45] B.H. Mackay, J.G. Downes, The kinetics of water-vapour soprtion in wool: Part II: Results obtained with an improved soprtion vibroscope, The Journal of the Textile Institute, 60, 378-394 (1969)

[46] I.C. Watt, Kinetic studies of the wool-water system – Part I: The influence of water concentration, Textile Res. J., 30, 453-460 (1960)

[47] K. Kulasinski, S. Keten, S.V. Churakov, R. Guyer, J. Carmeliet, D. Derome, Molecular mechanism of moisture-induced transition in amorphous cellulose, ACS Macro Lett., 3, 1037-1040 (2014)

[48] P. Coussot, Scaling approach of the convective drying of a porous medium, Eur Phys J B, 15, 557‑566 (2000). https://doi.org/10.1007/s100510051160

[49] B.N.J. Persson, Side-leakage of face mask, Eur. Phys. J. E, 44, 75 (2021)

[50] S. Verma, M. Dhanak, J. Frankenfield, Visualizing the effectiveness of face masks in obstructing respiratory jets, Phys. Fluids, 32, 061708 (2020)

[51] R. Vallabh, P. Banks-Lee, A.F. Seyam, New Approach for Determining Tortuosity in Fibrous Porous Media, Journal of Engineered Fibers and Fabrics, 5, 7–15 (2010). doi: 10.1177/155892501000500302.

[52] J. Crank, *The mathematics of diffusion*, Oxford Science Publication, Oxford, 1975